Journal of Fluorescence
https://doi.org/10.1007/s10895-023-03546-z

RESEARCH

# Luminescent Properties of β-(hydroxyaryl)-butenolides and Fluorescence Quenching in Water

**Beatriz Miorin Finêncio[1] · Fernanda Amorim Santos[1] · Renato Luis Tame Parreira[2] · Renato Pereira Orenha[2] · Sandro Marcio Lima[3] · Luis Humberto Cunha Andrade[3] · Maryleide Ventura[3] · Rosangela da Silva de Laurentiz[1]**

Received: 26 September 2023 / Accepted: 7 December 2023


**Abstract**
This work describes the luminescent properties of the new compound β-(hydroxyaryl)-butenolides recently discovered. The compounds were subjected to UV–Vis absorption and fluorescence analyzes when diluted in different solvents. Through the results, it was possible to observe that the β-hydroxyarylutenolides have two absorption bands, one at 289–291 nm and the other with higher intensity at 328–354 nm. The emission band between 385–422 nm is observed under excitation at 324–327 nm. The compounds showed solvatochromism as a function of the analyzed solvent. In water, fluorescence quenching of all compounds occurs. Therefore, studies with compound containing the methylenedioxy group attached in phenyl ring were carried at different concentrations of water in DMSO. The decrease in the fluorescence intensity of this compound is linearly proportional to the increase in the amount of water in the DMSO, with a minimum detection volume of 0.028%. Quantum yields of three compounds were evaluated in different solvents, showing that the relationship between the structure of the compound and the solvent is essential for a high value. The fluorescence quantum yield was also measured by Thermal Lens Spectroscopy (TLS) using DMSO as the solvent, confirming the high value for the analyzed samples. Despite being preliminary, the studies revealed that these compounds have luminescent properties that could be applied in the development of chemical sensors for detecting water in DMSO.

**Keywords** Solvatochromism · Fluorescence quenching · Fluorescence quantum yield · Butenolides

## Introduction

In recent decades, numerous fluorescent small organic molecules have been studied for application in light-emitting devices and sensors of the most varied types, due to their lower cost compared to other materials and their structural versatility [1]. In these compounds, the rigid core can be changed to present specific properties by introduction of OH, NH, OR, and OAc groups, among others, especially in aromatic rings. This functionalization can provide compounds with a wide range of emissions in the visible region [2, 3]. In compounds with aromatic rings conjugated to unsaturated carbon chains electron delocalization occurs mainly by one-dimensional bond conjugation. However, functionalization in the aromatic rings can further mechanisms such as charge transfer, dimer formation, or internal proton transfer. These mechanisms can increase or decrease the fluorescence and are directly related to the position and nature of different groups attached in the base structure [4, 5, 6, 7, 8].

The fluorescence of many of these conjugated systems can be influenced by the solvent used in the solution. Solvatochromism is the term used to describe the significant impact of a solvent's polarity on the absorption and emission spectrum of a compound. The absorption and emission bands will appear at different wavelengths depending on the solvent's ability to either increase or decrease stabilization of the excited state [9, 10].

✉ Rosangela da Silva de Laurentiz
rosangela.laurentiz@unesp.br

[1] Faculdade de Engenharia de Ilha Solteira, Departamento de Física e Química, Universidade Estadual Paulista (Unesp), Ilha Solteira, SP, Brazil

[2] Núcleo de Pesquisas Em Ciências Exatas e Tecnológicas, Universidade de Franca, Franca, SP, Brazil

[3] Centro de Estudos em Recursos Naturais – CERNA, Universidade Estadual de Mato Grosso do Sul – UEMS, Dourados, MS 79823-351, Brazil

Published online: 09 January 2024

Compounds that display strong solvatochromism have attracted considerable attention due to their potential applications, especially as sensors [11]. The solvent can change the shift and suppress the emission bands, as observed by Santos et al. [6]. The authors observed that one of the synthesized naphthoquinolines display two fluorescence bands due to ESIPT mechanism. However, in water, the emission bands corresponding to the keto form was suppressed while the band corresponding to enol form was shifted to a higher wavelength as a result of the hydrogen bonding with the water [12]. Water can also cause fluorescence quenching by transferring resonant energy from the compound in its excited state to combined bands of O – H vibrations from the water that overlap with the fluorescence emission from the compound [13]. Fluorophores that absorb and emit in the red region between 600 and 900 nm, in the absence of other higher-speed processes, are likely to have their fluorescence suppressed in water. However, this process can also occur for fluorescent compounds that absorb at wavelengths shorter than 600 nm when the excited state is long-lived [13, 14]. Compounds that exhibit a fluorescence quenching mechanism in water have the potential targets to be used in the development of sensors for detecting water content in organic solvents [15].

The butenolide nucleus is found in a variety of natural and synthetic products (Fig. 1) that possess significant biological properties [16, 17, 18, 19]. As a result, several researchers have focused on developing new methods for synthesizing these compounds, not only to explore their biological properties, but also to investigate properties related to molecular structures [20, 21]. Despite their important biological properties, there is a lack of literature on their optical properties. They have a short carbonic chain and a rigid structure due to the connection between the butenolide ring and the phenyl ring, allowing for electron delocalization through one-dimensional bond conjugation [22]. Additionally, substituting the aromatic ring with electron-donating groups can enhance fluorescence and change the mechanism by which fluorescence occurs [23].

In this work, we investigated the optical properties of β-hydroxybutenolides (Fig. 2) which were previously by reaction between tetronic acid (**1**) and phenols (**2**) promoted by $BF_3.OMe_2$ [24]. We examined the luminescent properties of these compounds with the aims to contributing to the current demand in the search for light-emitting small organic molecules as targets in the development of luminescent materials, chemical sensors, and biological probes [25, 26].

For this study, three β-(hydroxyaryl)-butenolides were submitted to analysis of absorption, emission, solvatochromism, and fluorescence quantum yield.

## Experimental Procedure

### General Information

All solvents used in the preparation of solutions of compounds **3a**, **3b**, and **3c** have HPLC grade and were used without further purification. Studies on optical properties were carried out at room temperature using a Shimadzu spectrophotometer (Model UV-1800) for UV–Vis analysis

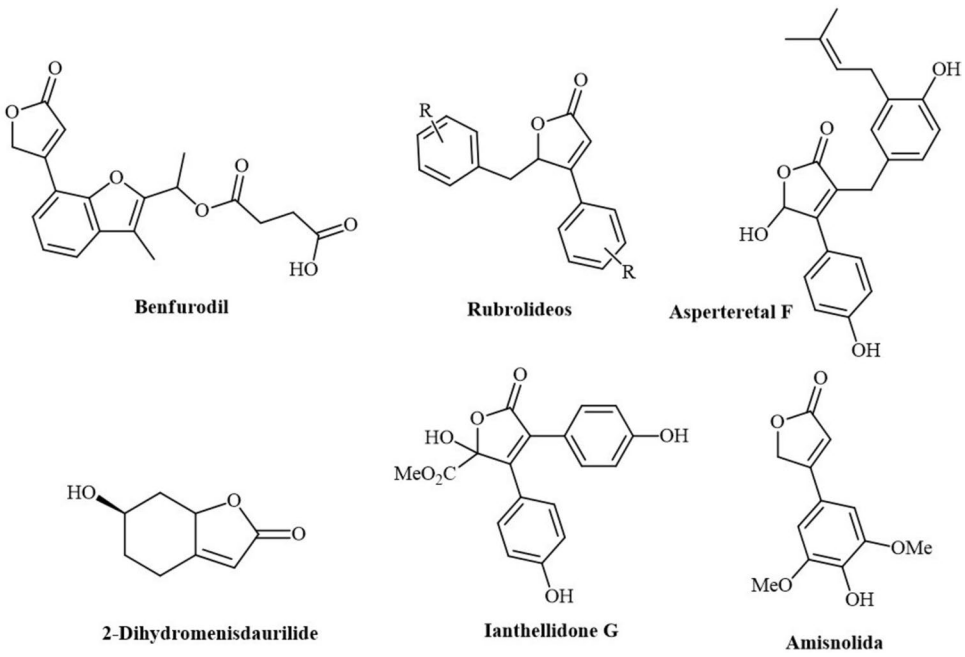


**Fig. 1** Natural and synthetic compounds containing the butenolide core

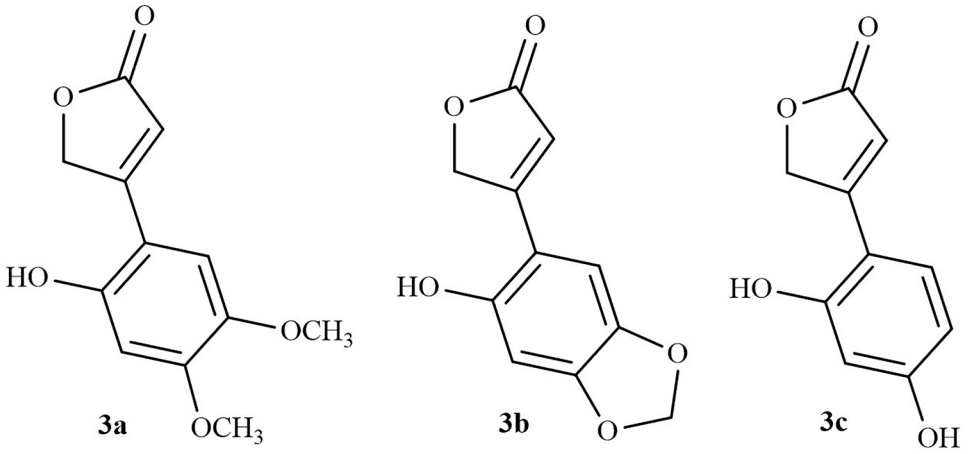


**Fig. 2** Structure of β-(hydroxyaryl)-butenolide **3a**, **3b**, and **3c**

and a Shimadzu spectrofluorophotometer (RF-6000) for fluorescence and quantum yield analyses.

## Spectroscopic Characterization

Absorption and emission analysis of the compounds **3a**, **3b**, and **3c** were carried out initially from DMSO solutions at $10^{-6}$ mol $L^{-1}$. Solvatochromism studies with derivatives **3a**, **3b**, and **3c** were carried out at room temperature from solutions in DMSO, chloroform, ethanol, water, and toluene at concentrations of $5 \times 10^{-6}$ mol $L^{-1}$ [6].

Studies on the effect of water concentration on optical properties were also carried out. Solutions of **3b** at different percentages of water (in DMSO) were prepared to maintain the final concentration at $5 \times 10^{-6}$ mol $L^{-1}$.

The fluorescence quantum yield ($\Phi_f$) was measured in several solvents through the integrated photoluminescence intensities and the absorbance values using as standard (*std*) the quinine sulfate ($\Phi = 0.546$) according to Eq. (1), wherein $A$ is defined as the absorbance of the excitation wavelength, $F$ as the area under the emission curve and $n$ is the refractive index of the solvents used. Subscript *std* is referent to data obtained for quinine sulfate [6].

$$\Phi_f = \Phi_{std} \times \frac{A_{std}F}{AF_{std}} \times \frac{n^2}{n_{std}^2} \quad (1)$$

The fluorescence quantum yield of **3a** and **3b** derivatives were also investigated using the dual-beam mode-mismatched configuration of the TLS in a time-resolved procedure. As schematized in Fig. 3(a), the TLS experimental setup is constituted of two laser beams, so that one of them is used to excite the material to create the thermal lens (TL) effect, while the second one, with low power, is used to probe the effect. Once the excitation laser beam has a Gaussian intensity profile, after the radiation is absorbed by the material, a temperature gradient from the beam center to the border can be observed, so that a radial temperature change, ΔT(r), creates a variation in the refractive index of the material [27, 28]. By aligning the probe laser beam to cross this heated region, it can be registered a phase shift in its wavefront in the far field, causing a divergence or a convergence of the beam. As usually done during the TLS procedure, it is possible to analyze the temporal response of this lens-like effect to determine the absorption coefficient ($\alpha$), the fluorescence quantum yield ($\Phi_f$) and thermal diffusivity (D) of semi-transparent materials.

To perform the experiments, a quartz cuvette with L = 5 mm thickness was used to insert the liquid samples. As shown in

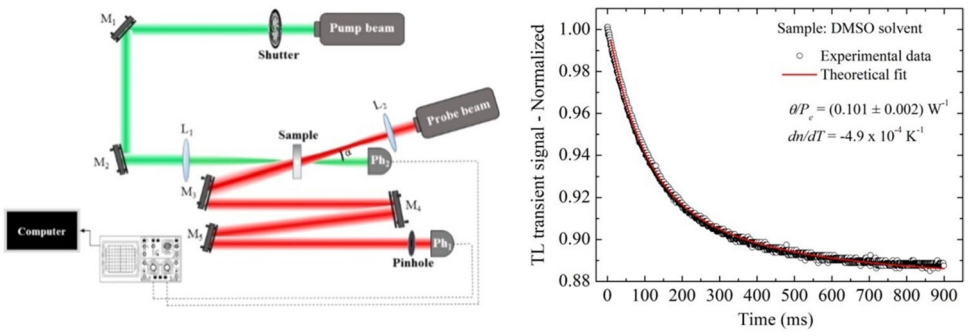


**Fig. 3** **(Left)** Experimental setup of the TLS, with *L's* indicating lenses, *M's* mirrors and *Ph's* the photodetectors. **(Right)** Characteristic TL transient signal for DMSO solvent obtained with $P_e = 6$ mW and the theoretical fit curve

Fig. 3, the cuvette is placed in the minimum beam waist ($w_{oe}$) of the excitation diode laser at $\lambda_{exc}=376$ nm. As probe laser was used a HeNe laser operating at 632.8 nm. Due the TL effect, the probe beam intensity registered in the far field as a function of time results in the typical normalized TL transient signal, I(t)/I(0). Figure 3(b) shows the curve obtained for the DMSO solvent.

The TL experimental data were fitted by using the theoretical model developed by Shen et al. [27], which express the on-axis transient intensity of the probe beam in the far field, *I(t)*, as:

$$I(t) = I(0)\left[1 - \frac{\theta}{2}tan^{-1}\left(\frac{2mV}{\left[(1+2m)^2+V^2\right]\left(\frac{t_c}{2t}\right)+1+2m+V^2}\right)\right]^2 \quad (2)$$

The term *I(0)* is the intensity when $t=0$ or $\theta=0$, and $m$ and $V$ are intrinsic geometric parameters from the probe and excitation lasers [28]. For the experiment were used $m=45.4$; $V=4.32$; and $L=5$ mm. In Eq. (2) $t_c = w_{oe}^2/4D$ is the TL characteristic time constant and $D$ ($cm^2\ s^{-1}$) is the thermal diffusivity. The amplitude of the TL signal is proportional to $\theta$, which is approximately the probe beam thermally induced phase difference, is given by:

$$\theta = -\frac{P_e \alpha L}{K\lambda_p}\varphi\frac{dn}{dT} \quad (3)$$

The $P_e\alpha L$ product corresponds to the absorbed power by the sample ($P_{abs} = P_e\alpha l$), with $P_e$ (W) being the excitation power, $\alpha$ ($cm^{-1}$) the absorption coefficient at the excitation wavelength, and $L$ (cm) the cuvette thickness; $\lambda_p$ (cm) is the probe wavelength and *dn/dT* ($K^{-1}$) is the thermo-optical coefficient [27, 28]. $K=\rho CD$ is the thermal conductivity ($Wcm^{-1}\ K^{-1}$), $\rho$ ($gcm^{-3}$) is the volumetric density of the sample, $C$ ($Jg^{-1}\ K^{-1}$) is the specific heat; and φ is proportional to the fraction of absorbed energy converted to heat in the material, which is given by:

$$\varphi = 1 - \Phi_f\left(\frac{\lambda_{exc}}{<\lambda_{em}>}\right) \quad (4)$$

in which $\lambda_{exc}$ is the excitation beam wavelength and $<\lambda_{em}>$ is the average emission wavelength obtained from the fluorescence spectrum [27, 28]. In this case, for the studied samples, $<\lambda_{em}> = 422$ nm.

The absorption coefficient of the samples at the excitation wavelength was determined through the relationship between the incident power (excitation power), $P_{in}$, and the transmitted power, $P_t$, given by:

$$\alpha = -\frac{1}{L}ln[\frac{P_t}{P_{in}(1-R)^2}] \quad (5)$$

in which R corresponds to the reflectance of the sample, $R = \left(\frac{n-1}{n+1}\right)^2$, where $n$ is the refractive index of the solvent used in the sample dilutions.

## Computational Methods

### UV–Vis Absorbance Spectra

The geometry optimizations of all compounds were performed without constraints and the vibrational frequencies were calculated using the BLYP [29, 30, 31] functional and Grimmes D3 dispersion correction with Becke-Johnson damping function (D3(BJ)) [32] in combination with the Def2-TZVP basis set [33]. The RIJCOSX [34, 35] approximation has been used to speed up the calculations performed. Coulomb integrals were approximated with the RI-J [34] approach using the Def2/J auxiliary basis set [36]. The absence of imaginary eigenvalues in the Hessian matrix indicated that all optimized geometries correspond to the minima of energy on the potential energy surface. The UV–Vis spectrum of the compounds investigated has been calculated using the STEOM-DLPNO-CCSD [37, 38] method along with the Def2-TZVP basis set. The Def2-TZVP basis set also was used as an auxiliary basis set. The RIJCOSX approximation also was employed here to speed up these calculations. The $H_2O$ or DMSO solvation has been considered using the solvation model based on density (SMD) [39]. All calculations were done using the ORCA program package [40].

### Theoretical Investigation of the Fluorescence Suppression in Water

The geometry optimizations of all compounds in ground state or the first excited state were performed without constraints and the vibrational frequencies were calculated using the BLYP [29, 30, 31] functional and Grimmes D3 dispersion correction with Becke–Johnson damping function (D3(BJ)) [32] in combination with the Def2–TZVP [33] basis set. The DMSO or water solvation was implicitly included with the polarizable continuum model (PCM) through the integral equation formalism variant (IEFPCM) [41]. Vibrational analyzes for all optimized geometries confirm that they are all energy minima at the computational model applied here. The dipole moment, and the energy values related to the highest occupied molecular orbital (HOMO) and the lowest unoccupied molecular orbital (LUMO) have been selected. These calculations were made through of the Gaussian 16 (Revision B.01) software [42].

## Results and Discussion

### Spectroscopic Characterization

The photophysical properties of derivatives **3a**, **3b**, and **3c** were studied using UV–Vis absorption and fluorescence spectroscopy. These derivatives exhibited two absorption bands with maximum absorbance wavelengths ranging from 328 to 354 nm when DMSO was used as the solvent (Fig. 4).

The maximum absorbance position, observed when the samples were diluted in DMSO was used to excite the samples for emission spectra determination (Fig. 5). The resulting photophysical data from the analysis are presented in Table 1.

The compounds exhibited emission bands in the violet-blue range, with maximum intensity values recorded at 385 nm for **3c**, 421 nm for **3a**, and 422 nm for **3b**. Additionally, a shift towards longer wavelengths (bathochromic shift) in the emission band of 3a and 3b compared to 3c was observed due to the presence of the more substituent groups in these two derivatives, contributing to increasing the stability of the excited state [43].

All derivatives share the β-(hydroxyaryl)-butenolide fluorophore and the difference in their absorption spectra are due to the nature and quantity of the different groups attached to this fluorophore. When changes occur in the fluorophore, it is expected that the characteristic energy of a transition and the wavelength of the absorbed radiation will also change. Derivatives **3a** and **3b** have absorption bands with similar intensity and a slight variation in the $\gamma_{max}$ value. However, derivative **3c** has an absorption band at a shorter wavelength. This is because derivative **3**c only has one additional

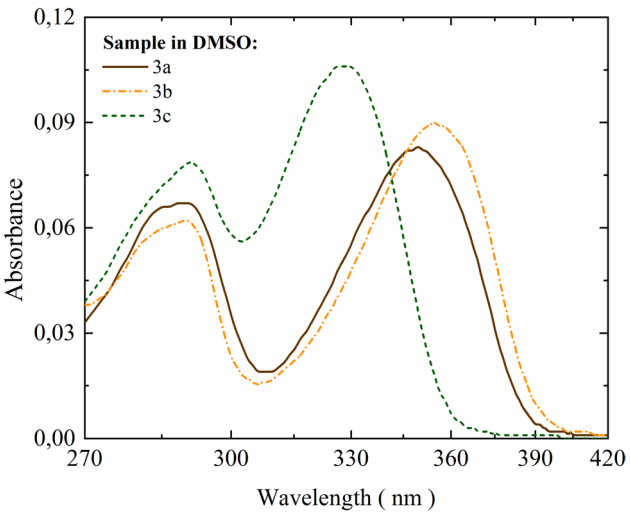


**Fig. 4** Absorbance spectra of **3a**, **3b**, and **3c** in DMSO solutions at a concentration of $5\times10^{-6}$ mol $L^{-1}$

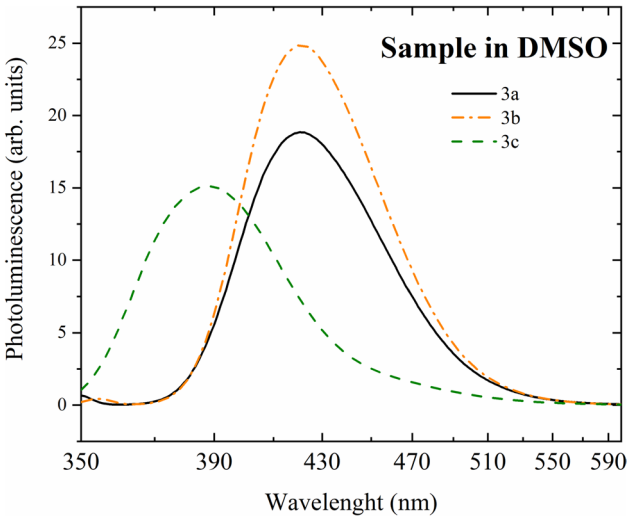


**Fig. 5** Emission spectra of compounds **3a**, **3b**, and **3c** in DMSO at $5\times10^{-6}$ mol $L^{-1}$

substituent attached to the phenyl ring (OH group), while the other derivatives, have two more electron donating groups. Derivative **3a** has two $OCH_3$ groups, and derivative **3b** has a methylenedioxy group -O-$CH_2$-O- attached to the phenyl ring by the two oxygens (Fig. 2). These substituents possess non-bonding electrons (*n* electrons) that, through resonance, can increase the length of the π-electron system. This behaviour is observed when a hydrogen on the aromatic ring is replaced by electron-donating groups, causing the substituted compound to exhibit absorption at longer wavelengths compared to the unsubstituted compound [44]. The presence of any substituent, whether electron-donating or electron-withdrawing, alters the absorption and emission of the fluorophore. The bands can be shifted to longer wavelengths depending on the interaction that the substituent has with the fluorophore nucleus, such as the extent of conjugation or increased intramolecular charge transfer (ICT) [45].

Stokes shift values do not indicate internal proton transfer, so this kind of mechanism is when Stokes shifts are greater than 100 nm [6, 46]. However, these compounds have structures that, after energy absorption, reach an excited state where charge transfer occurs from the aromatic ring to the

**Table 1** Photophysical data for **3a**, **3b**, and **3c** in DMSO at $5\times10^{-6}$ mol $L^{-1}$. $\lambda_{ab}$ and $\lambda_{em}$ are the maximum position of the absorbance and emission wavelengths, respectively

| Sample | $\lambda_{ab}$ (nm) | | $\lambda_{em}$ (nm) | Δλ Stokes (nm) | $\Phi_f$ |
|---|---|---|---|---|---|
| | Band 1 | Band 2 | | | |
| **3a** | 290 | 354 | 421 | 73 | 0.59 |
| **3b** | 289 | 348 | 422 | 68 | 0.94 |
| **3c** | 291 | 328 | 385 | 57 | 0.25 |

butenolide ring, and this charge transfer may explain the observed emission [43].

## Fluorescence Quantum Yield

Fluorescence quantum yields ($\Phi_f$) of compounds **3a**, **3b**, and **3c** were performed using quinine sulfate as a standard, which has a quantum yield of 0.54 in 1 M $H_2SO_4$ solution. $\Phi_f$ values of the synthesized derivatives measured in the DMSO solution were highly influenced by the substituents on the aromatic ring. The results showed that compound **3b** has $\Phi_f$ of 0.94, which indicates that practically all the absorbed energy is emitted with little energy being dissipated in non-radioactive processes [6]. The $\Phi f$ of compounds **3a** and **3c** were 0.59 and 0.25, respectively. Derivative **3b** possesses a methylenedioxy group attached to the phenyl ring, forming a 5-membered ring with the two carbons of the phenyl ring. This results in a more rigid structure that reduces losses caused by non-radioactive processes. In **3a**, the presence of two $OCH_3$ groups attached in phenyl ring leads to a decrease in quantum yield, possibly due to deactivation caused by non-radioactive process resulting from the rotation of these groups [47]. However, the quantum yield of **3a** is still higher than that of **3c**. In **3c**, the other substituent attached to the phenyl ring is an OH group, likely contributing to the lowest quantum yield among the three derivatives. During the fluorescence process, the interaction between a photon and a molecule generates the excited molecule $A + h\gamma \rightarrow A^*$. Subsequently, various non-radioactive processes can compete with light emission and reduce the quantum yield. These processes can occur simultaneously and depend on the molecular structure of the fluorophore. Therefore, elucidating which of these processes occur in **3c** is a challenging task. However, it is plausible to hypothesize that the second hydroxy group attached to the phenyl ring of **3c** may interfere with the charge transfer process through intermolecular hydrogen bonding.

## Fluorescence Quantum Yield by Thermal Lens Spectroscopy

In order to better investigate the luminescent properties of samples **3a** and **3b,** which were diluted in DMSO at a concentration of $5 \times 10^{-6}$ mol $L^{-1}$ concentration, TLS measurements were conducted. As shown in Fig. 3, a laser with a wavelength of 376 nm was used to excite the sample during TLS measurement. This wavelength is adequate for promoting electrons in samples **3a** and **3b**, but not in sample **3c** (as seen in the absorption shown in Fig. 4). This explains why sample **3c** was not investigated. First, the values of the absorption coefficient ($\alpha$) were obtained for each sample, by calculating the ratio between transmitted and incident power at 376 nm, $P_t/P_{in}$, using Eq. (4). Thus, the following values were found: 0.0132 $cm^{-1}$ for the DMSO solvent, 0.1481 $cm^{-1}$ for sample **3a,** and 0.1421 $cm^{-1}$ for sample **3b**. It is important to mention that the sample 3c was not measured using this method because its absorbance at 376 nm is very low (see Fig. 4).

In the TLS measurements, transient signals were obtained as a function of the excitation power ($P_e$) for each sample, as shown in Fig. 3(b). The transients (experimental data) were fitted with Eq. (1) to obtain the parameters $\theta$ and $t_c$. The absorbed power was determined based on values of $P_e$, $\alpha$ and $L$ (5 mm). The $\theta/P$ abs ratio of the samples was obtained from the data of $\theta$ as a function of $P_{abs}$, as shown in Fig. 6. This ratio, known as $\Theta$, was mathematically manipulated according to Eq. (2):

$$\Theta = \frac{1}{K\lambda_p}\varphi\left(\frac{dn}{dT}\right) \tag{5}$$

From Eq. (5), it was found $\Theta$ for the reference sample (DMSO solvent), $\Theta_{ref}$, and for the samples diluted in DMSO (**3a** and **3b**), $\Theta_{sample}$. In this case, the reference sample does not have fluorescence, i.e., all the energy absorbed by this sample is converted into heat, $\varphi = 1$.

Thus, the ratio between $\frac{\Theta_{sample}}{\Theta_{ref}}$ gives us the value of $\varphi$ for each sample, indicating the amount of energy absorbed that was converted into heat. From the values of $\varphi$ for each sample, it was possible to find $\Phi_f$, by Eq. (3). Table 2 summarizes the results of the fluorescence quantum yield found for the samples **3a** and **3b**.

From the results, it is possible to note that the **3b** sample presents a higher quantum yield of 95%, which is in agreement with the obtained photophysical data (94%). The **3a** sample, on the other hand, showed a quantum yield of 74%, slightly higher than the value of 59% obtained through the photophysical data (59%).

## Computational Study of the UV–Vis Absorbance Spectra

The main electronic transitions presented in the UV–Vis absorbance spectra of the compounds **3a**, **3b**, and **3c** solvated in DMSO or water were identified from theoretical calculations (Table 3, Figs. 7 and S1).

Due to the similarity of the molecular orbitals of the compounds studied in DMSO or water, the main molecular orbitals obtained for the molecules analyzed solvated in water have been organized in the supplementary material. Firstly, it is important to highlight that there are close values of the wavelengths obtained from experimental and theoretical data for the two main bands present in the UV–Vis absorbance spectra of the investigated compounds. Additionally, the main wavelength values obtained in the UV–Vis absorbance spectra of the compounds **3a**, **3b**, and **3c** solvated in

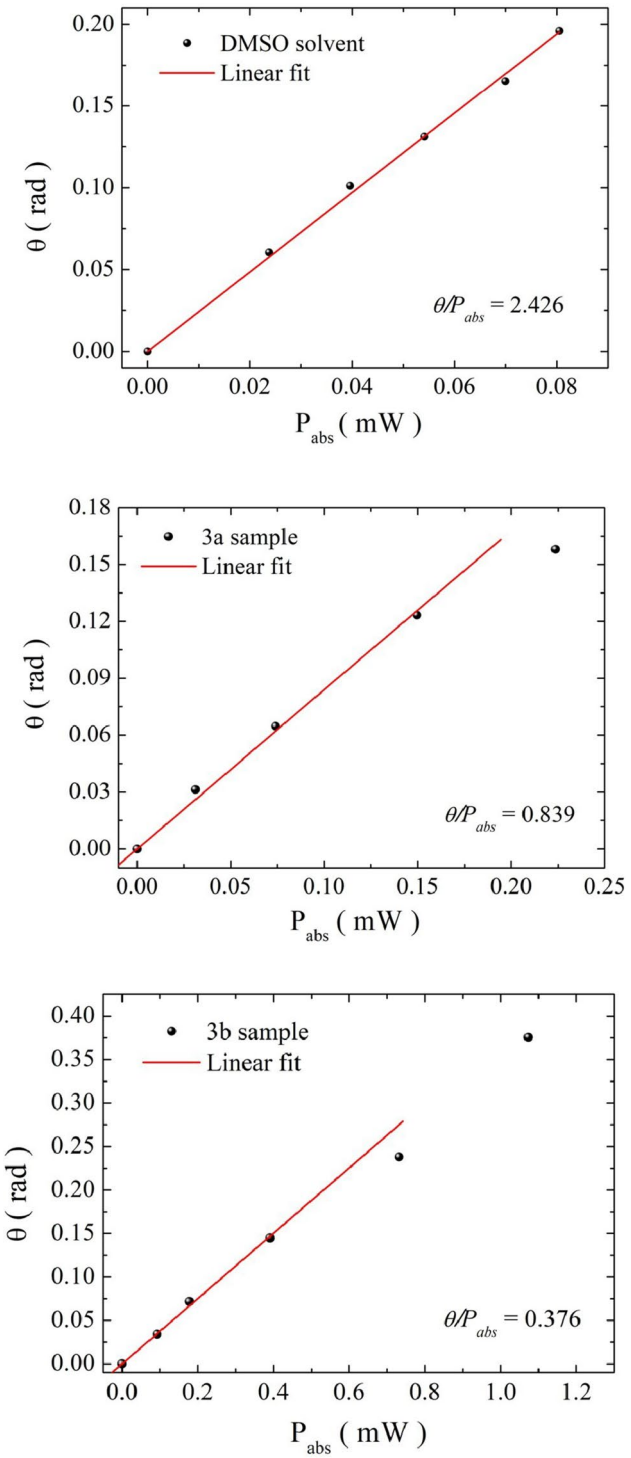


**Fig. 6** $\theta$ in function of $P_{abs}$ for the DMSO solvent, **3a** sample and **3b** sample

DMSO are similar to those obtained in water. The band close to 280 nm in structures **3a** and **3b** is mainly associated with the electronic transition between the molecular orbitals HOMO-1 and LUMO (50–56%). On the other hand, in structure **3c**, there are three main electronic transitions:

**Table 2** Results of $\Theta$, $\varphi$ and $\Phi_f$ for the samples studied

| Sample | $\Theta(mW^{-1})$ | $\varphi = \frac{\Theta_{sample}}{\Theta_{ref}}$ | $\Phi_f$ |
|---|---|---|---|
| DMSO | 2.43 ± 0.09 | ----- | ----- |
| **3a** | 0.84 ± 0.04 | 0.34 ± 0.02 | 0.74 ± 0.07 |
| **3b** | 0.38 ± 0.02 | 0.15 ± 0.01 | 0.95 ± 0.09 |

i) HOMO-1 → LUMO (31–39%); ii) HOMO → LUMO (20–29%), and iii) HOMO → LUMO + 1 (30–31%). The band close to 320 nm is mainly composed of the electronic transition HOMO → LUMO (66–86%) in all the studied structures. This band is preferentially shifted to the UV region in structure **3c** compared to compounds **3a** and **3b**.

## Solvatochromism Studies

After the study in DMSO, these compounds were also analyzed in other solvents to verify the influence of these solvents on their photophysical properties. For this study, the compounds were dissolved in DMSO, ethanol, water, chloroform, ethyl acetate, and toluene at a final concentration of $5 \times 10^{-6}$ mol $L^{-1}$. The aqueous solutions of the compounds were prepared by diluting a concentrated solution of DMSO with water, resulting in a final concentration of DMSO in the aqueous solution of 0.12%. Regarding the absorption of **3a**, **3b**, and **3c** in the different solvents, it was observed that in more polar solvents the bands appear at higher wavelengths (Fig. 8).

In the water, a third band superimposed on the second appears at 400 nm in the spectrum of **3a** and **3b,** while in **3c** this band appears at 361 nm. This third band can be attributed to the low solubility of compounds in water as it disappears at lower concentrations of water in the DMSO. The intensity of the bands was also affected by the nature of the solvent (Fig. 8). The emission spectra and data from the solvatochromism study are shown in Fig. 9 and in Table 4.

Some changes are seen in the emission spectra when a decrease occurs in the dipole moment of the solvent, so the emission spectrum undergoes a hypsochromic shift, as in toluene and chloroform [6].

The results showed that solvent characteristics an influence the fluorescence of **3a**, **3b**, and **3c**. Toluene and chloroform, which are less polar solvents, stabilize the excited state less. This causes a hypsochromic effect, resulting in emission at shorter wavelengths. In polar solvents, bathochromic effect was observed. This is likely due to greater stabilization of the excited state, leading to a decrease in energy and a shift in the emission band to longer wavelengths. This observation aligns with results obtained by Santos et al. [6]. These results indicate that the fluorescence process involves allowed electronic transitions of the $\pi \rightarrow \pi^*$ type [6, 40, 46].

**Table 3** Main electronic transitions are present in the UV–Vis spectrum of the compounds **3a**, **3b**, and **3c** solvated in DMSO or $H_2O$

| Compound (Solvent) | Band 1 | Band 2 |
|---|---|---|
| 3**a** (DMSO) | 280[a] [HOMO-1 → LUMO (50)[b]] | 326 [HOMO → LUMO (73)] |
| 3**a** ($H_2O$) | 287 [HOMO-1 → LUMO (55)] | 332 [HOMO → LUMO (76)] |
| 3**b** (DMSO) | 283 [HOMO-1 → LUMO (50)] | 336 [HOMO → LUMO (82)] |
| 3**b** ($H_2O$) | 289 [HOMO-1 → LUMO (56)] | 342 [HOMO → LUMO (86)] |
| 3**c** (DMSO) | 277 [HOMO-1 → LUMO (31); HOMO → LUMO (29); HOMO → LUMO + 1 (31)] | 308 [HOMO → LUMO (66)] |
| 3**c** ($H_2O$) | 282 [HOMO-1 → LUMO (39); HOMO → LUMO (20); HOMO → LUMO + 1 (30)] | 314 [HOMO → LUMO (74)] |

[a]Wavelength in nm

[b]Weight (in %) of the electronic transition between the molecular orbitals

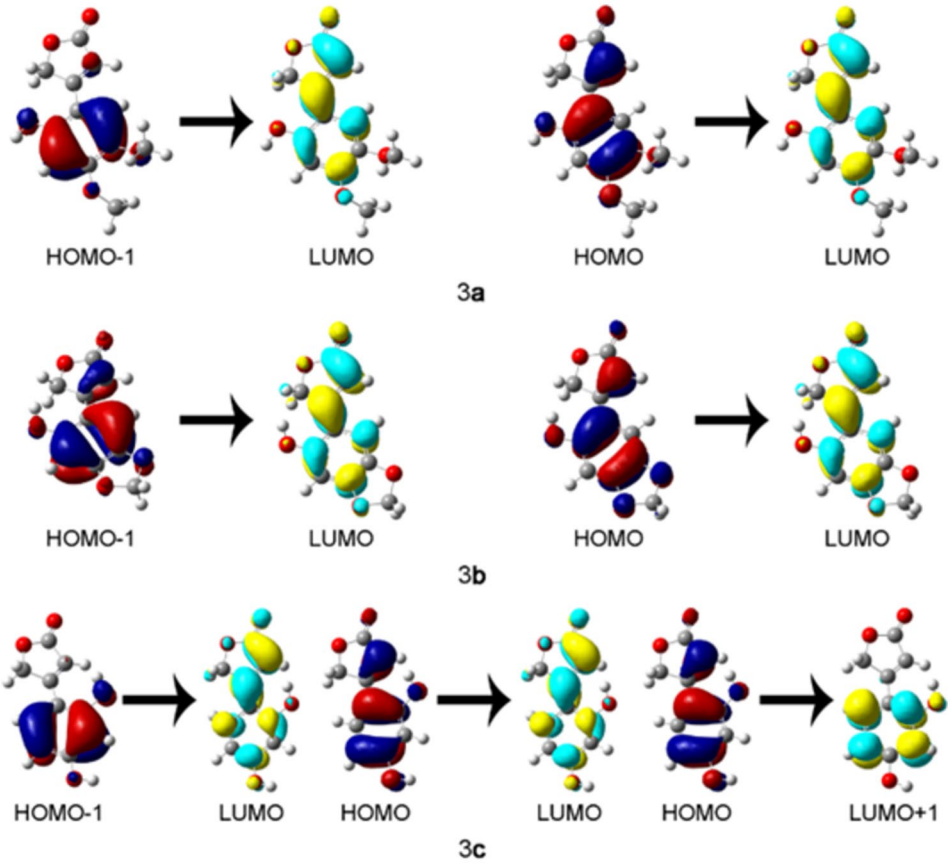


**Fig. 7** Main electronic transitions between the molecular orbitals of the compounds **3a**, **3b**, and **3c** solvated in DMSO

When the most polar solvent stabilizes the excited state more than the ground state, the separation between the energies of the ground and excited states is reduced, causing a shift in the absorption spectrum towards the red [46]. This phenomenon is known as solvatochromism and the extent of this shift is determined by the change in the molecule's dipole moment during the excitation process [46].

The emission spectra of **3a** and **3b** show similar displacement (nm) and intensity of bands in the same solvents. However, in ethanol, the intensity of the bands of 3c is altered, with twice the intensity compared to **3a** and **3b**. This observation suggests that compound **3c** in ethanol remains in the excited state for a longer period, allowing fluorescence to be observed for a longer time. In water, the emission band of all three derivatives are suppressed. This suppression is likely due to functional groups present in these compounds undergoing protonation in water, preventing internal charge transfer (ICT) and leading to the suppression of fluorescence [47]. A similar mechanism has been described for naphthol, which also experiences fluorescence quenching in water [48]. Other mechanisms, such as the formation of non-fluorescent species through

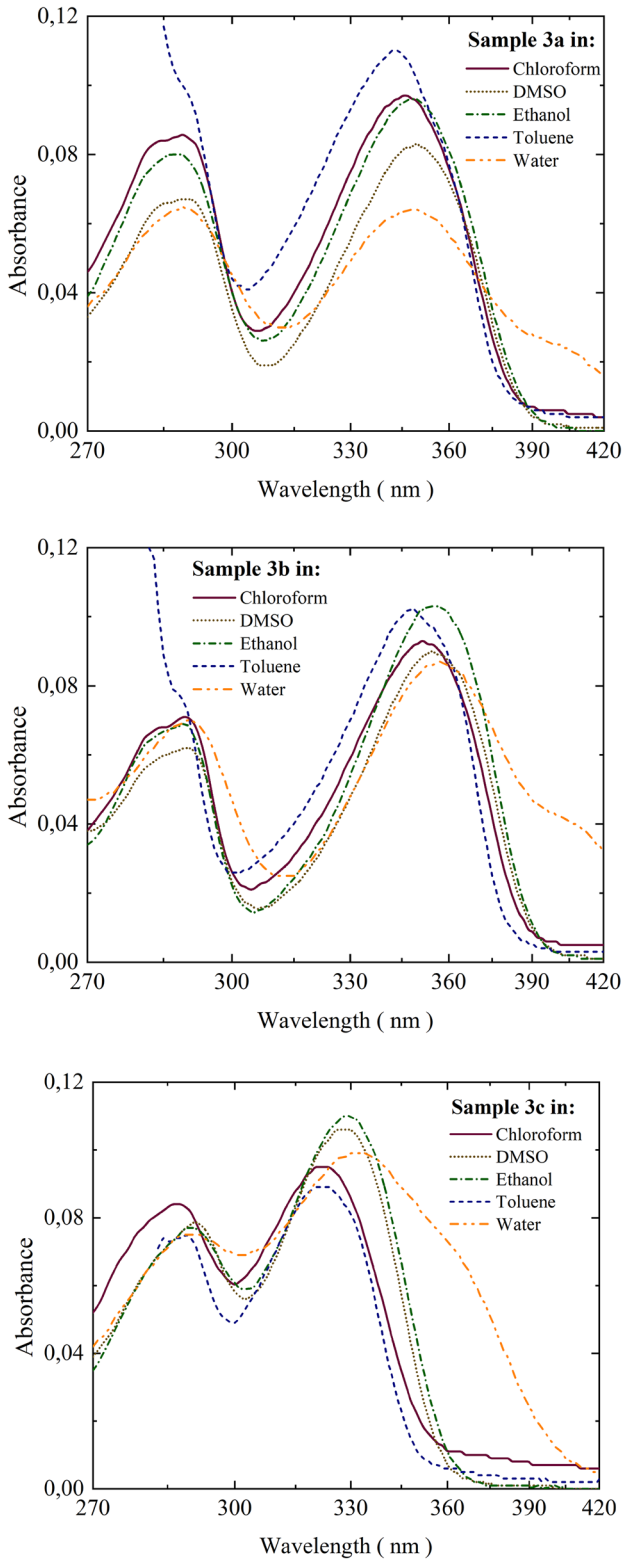


**Fig. 8** Absorbance spectra of **3a**, **3b**, and **3c** in different solvents at the concentration of $5 \times 10^{-6}$ mol $L^{-1}$

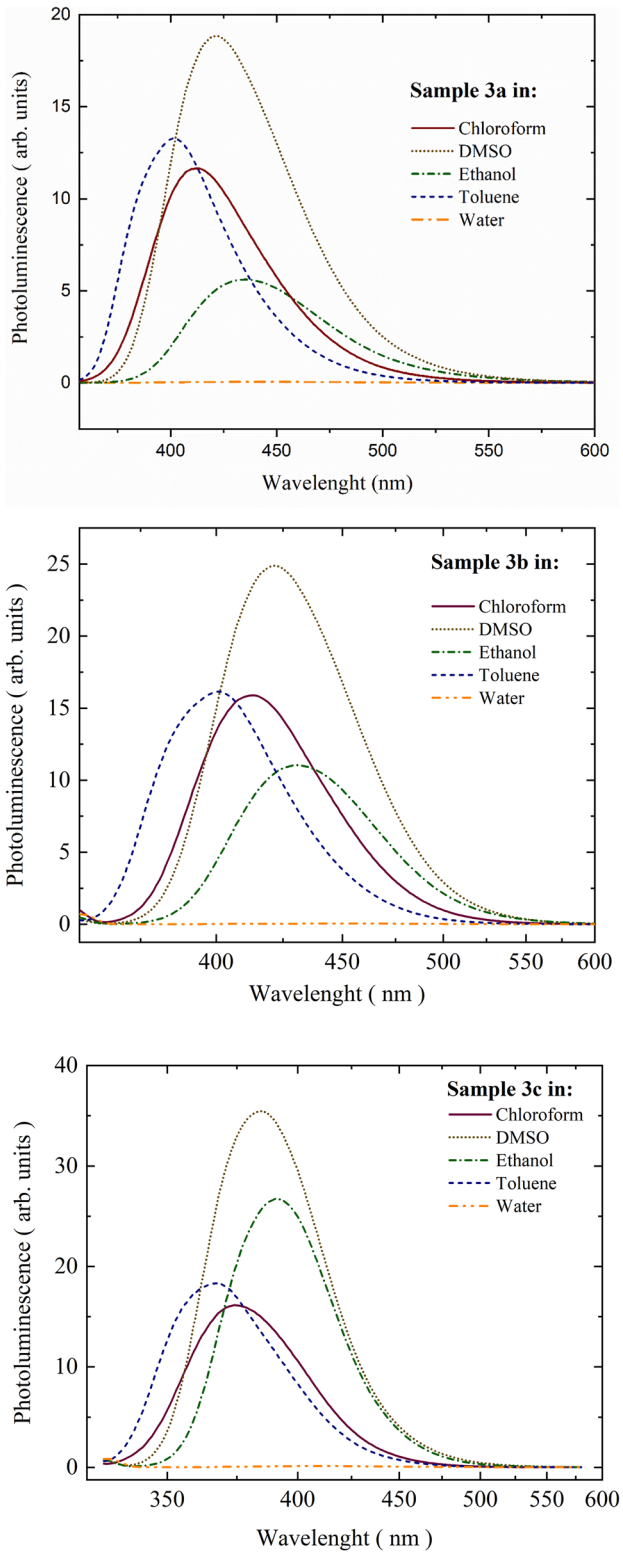


**Fig. 9** Emission spectra of **3a**, **3b**, and **3c** in solvents of different polarities at a concentration of $5 \times 10^{-6}$ mol $L^{-1}$

**Table 4** Photophysical data of **3a**, **3b**, and **3c** in solvents of different polarities. λ are in nm

| Solvent | Compounds | | | | | | | | | | | |
|---|---|---|---|---|---|---|---|---|---|---|---|---|
| | **3a** | | | | **3b** | | | | **3c** | | | |
| | $\lambda_{ab}$ | $\lambda_{em}$ | $\Delta\lambda_{St}$ | $\Phi_f$ | $\lambda_{ab}$ | $\lambda_{em}$ | $\Delta\lambda_{St}$ | $\Phi_f$ | $\lambda_{ab}$ | $\lambda_{em}$ | $\Delta\lambda_{St}$ | $\Phi_f$ |
| DMSO | 289; 348 | 422 | 74 | 0.59 | 290; 354 | 422 | 68 | 0.94 | 291; 328 | 388 | 60 | 0.26 |
| Chloroform | 289; 345 | 414 | 69 | 0.72 | 289; 352 | 413 | 61 | 0.67 | 287; 324 | 380 | 56 | 0.23 |
| Ethanol | 287; 349 | 436 | 87 | 0.21 | 289; 354 | 431 | 77 | 0.31 | 289; 329 | 391 | 62 | 0.35 |
| Water | 288; 349 | 399 | 50 | 0.00 | 288; 354 | 460 | 106 | 0.00 | 287; 323 | 407 | 84 | 0.00 |
| Toluene | 279; 343 | 401 | 58 | 0.56 | 288; 349 | 401 | 52 | 0.04 | 289; 323 | 368 | 45 | 0.16 |

hydrogen bonding between water molecules and molecules of the target compound [12].

Computational calculations performed by other authors have shown that for certain types of fluorescent compounds which are already in hydrogen bonding with the solvent before light absorption, the hydrogen bond is strengthened after transitioning to the excited state. This strengthening leads to a rapid transfer of electrons from the solvent to the chromophore resulting in the suppression of fluorescence [49]. However, experimental data suggest that after transitioning to the excited state, this hydrogen bond may weaken, leading to the suppression of fluorescence and a decreased in quantum yield [50].

The hydrogen bond donor solvents have ability to stabilize charges, making it difficult for charge transfer to occur to electron acceptor groups in water. However, this effect is not observed in ethanol. Although ethanol is also a protic solvent, the strength of this hydrogen bond is weaker compared to water. This weaker bond strength may explain why fluorescence suppression does not occur in ethanol [12]. Another potential mechanism that could be involved in the suppression fluorescence in water is aggregation-causing quenching (ACQ), which is favored by strong hydrophobic interactions [51].

The **3c** derivative showed the lowest solvatochromism (Table 4) and emission bands at shorter wavelengths. Compounds **3a**, **3b**, and **3c** emit light in the blue-violet region when excited by a UV lamp at 365 nm (Fig. 10).

The emission in the violet region is more pronounced in a nonpolar solvent such as toluene, with the most intense emission occurring in ethanol and DMSO for the three compounds. The nature of the solvent also affects the quantum yield, with **3b** showing a $\Phi_f$ of 0.94 in DMSO, but this value decreasing in other solvents. Derivative **3c** exhibited the highest $\Phi_f$ value in ethanol, while the nature of the solvent had less effect on 3a. In water, the fluorescence suppression process, result in a $\Phi_f$ value of zero for all three compounds (Table 4, Fig. 10).

The fluorescence quantum yield ($\Phi_f$) plays a significant role in many fluorescence-based applications and in the **3a**, **3b**, and **3c** derivatives, it is influenced by solvent and by substituent groups in the phenyl ring. The $\Phi_f$ is dependent on the interaction between compounds and solvents. DMSO, a polar solvent, can receive hydrogen bonds and interact with the compounds, greatly stabilizing the excited state and furnishing a higher quantum yield (Table 4). Chloroform which is not able to donate or receive hydrogen bonds, is still able to stabilize the excited state, but the solute–solvent interactions are weak, resulting in a greater *Φf*. In toluene, a is nonpolar solvent, the interactions between the compound and solvent are weak leading to higher quantum yield. Ethanol forms a hydrogen bond with the OH group of the phenol moiety, interacting with the compound and decreasing the

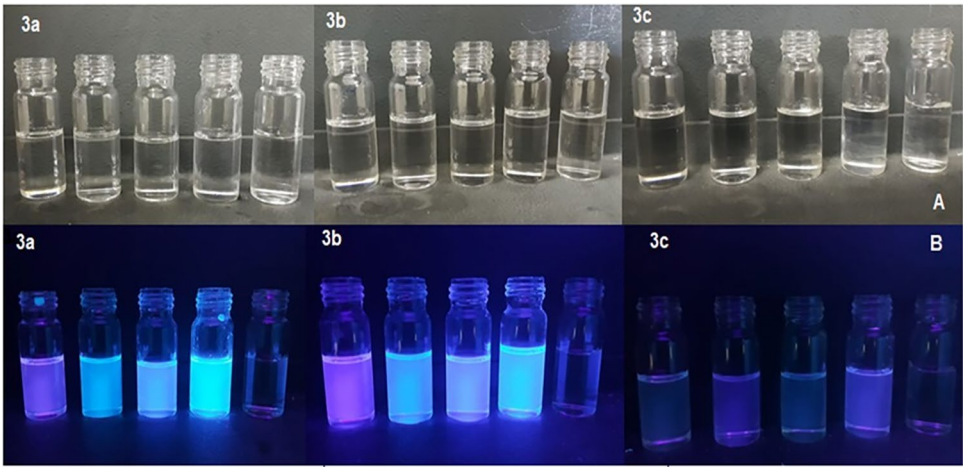


**Fig. 10** Photographs of **3a**, **3b**, and **3c**: before (upper side) and during (underside) excitation using a UV lamp at 365 nm. From left to right: toluene, ethanol, chloroform, DMSO, and water

*Φf*. In water, where the interaction is stronger, the fluorescence of the three compounds is suppressed ($\Phi_f = 0$) However, the high values of $\Phi_f$ observed in DMSO, chloroform, and toluene are essential for organic molecules to be used in sensors. The substituents in the phenyl ring of derivative **3a**, **3b**, and **3c** are not the same and possibly stabilize or destabilize the electronic density of the aromatic ring in different ways [6].

## Study of the Fluorescence Suppression in Water

Solvatochromism is a characteristic exhibited by certain fluorescent compounds as a result of intermolecular interactions with the solvent, which in turn alters their photophysical properties. This solvatochromism allows these fluorescent compounds to be as probes for analysis of solvent mixtures, as well as sensors for detecting the presence of water in polymeric matrices used in gaseous chromatography among others applications [46, 52].

The results demonstrate the solvatochromism of the compounds under evaluation, with the noticeable color change from toluene (violet) to DMSO (blue). Additionally, there was a suppression of fluorescence in water, indicating the potential use of these compounds as sensors for detection of water in organic solvents. The analysis of fluorescence suppression in water was conducted with **3b**, which exhibited a higher quantum yield. Fluorescence suppression can occur through various mechanisms or a combination of mechanisms [53, 54]. In a dynamic collision suppression mechanism, there is no change in the spectrum, as it only affects the excited states of the fluorophores, while the formation of complexes (static suppression) often results in a disturbance in the absorption spectrum. In this way, it is possible to suggest that the suppression mechanism for **3a**, **3b**, and **3c** occurs by collision since there is no change in the absorbance spectrum as a function of the variation in the amount of water as shown in Fig. 11 [54].

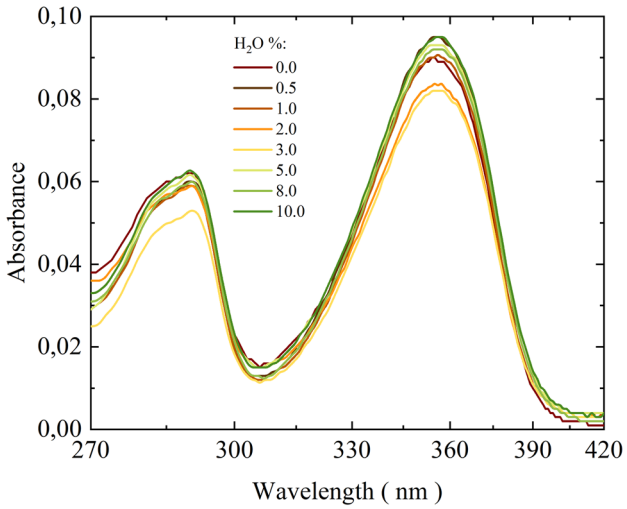


**Fig. 11** Absorbance spectra of **3b** at different percentages of water in the DMSO solution

Analyses of absorbance were performed in triplicate with water concentrations ranging from 0.0% to 10% in DMSO solution (Table S1). However, only one analysis of each water percentage was presented to avoid interferences with the visualization of the Fig. 11.

The concentration of **3b** in all analysis was maintained at $5 \times 10^{-6}$ mol $L^{-1}$. The fluorescence spectrums of **3b** shows an emission band that decreases with an increasing amount of water content (0 to 10%) (Fig. 12a) and a soft bathochromic shift is observed (from 422 to 428 nm). In the detection interval range from 1.00%–10.00% (v/v%), there is an obvious linear correlation between fluorescence intensity and water percentage. The corresponding linear regression equation for this interval can be expressed as $y = 405282.746 - 13610.140 \times$ where $R^2 = 0.985$ (Fig. 12b). The linearity of the analysis allows the use of this equation to determine the water content in DMSO with detection limit of 0.028% [54].

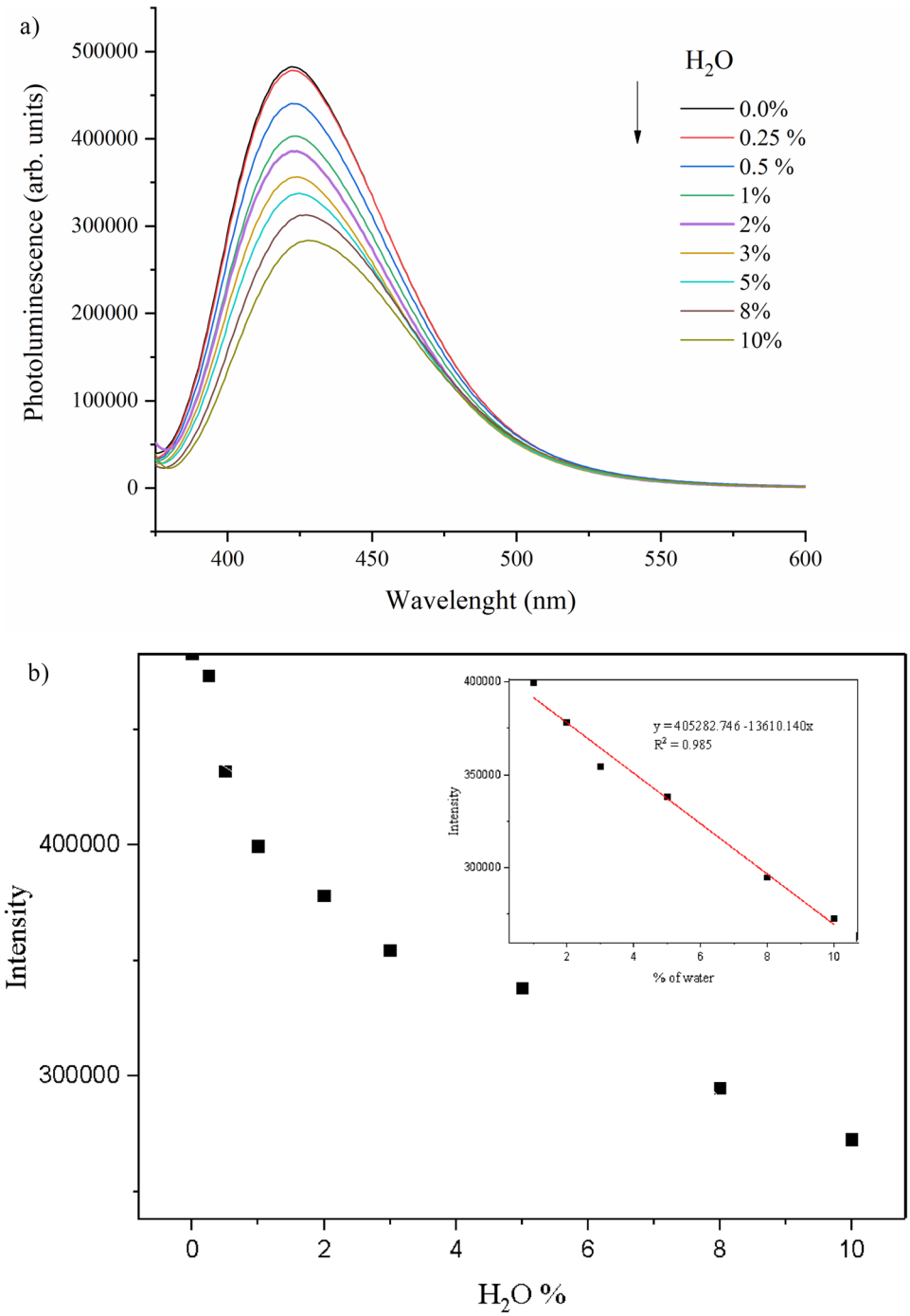


**Fig. 12** **a** spectra of **3b** were recorded at various percentages of water in the DMSO solution. The concentration of **3b** in all analyses was held constant at $5 \times 10^{-6}$ mol $L^{-1}$, with excitation at 354–357 nm **b** the relationship between fluorescence intensity and water percentage, was examined, with the corresponding fitting curve shown in the inset

Theoretical calculations were conducted to elucidate the suppression of fluorescence in water (fluorescence quenching). The parameters used to analyze the fluorescence quenching included the dipole moment from the ground state ($\mu_g$) to the excited state ($\mu_e$) and the energy gap between the frontier molecular orbitals present in the ground state. The frontier molecular orbital distributions of **3b** was calculated using density functional theory (DFT) with the B3LYP [32, 33] method in both DMSO and water as shown in Fig. 13. In DMSO, the highest occupied molecular orbital (HOMO) is delocalized on the aromatic ring and its substituents, while the lowest unoccupied molecular orbital (LUMO) is delocalized on the butenolide moiety. In water, the HOMO and LUMO are practically overlapping and the charge is delocalized over the entire molecular skeleton.

The molecular orbital distribution indicates that the electronic transition resembles an intern charge-transfer (ICT) transition from HOMO to LUMO in DMSO. In this solvent,

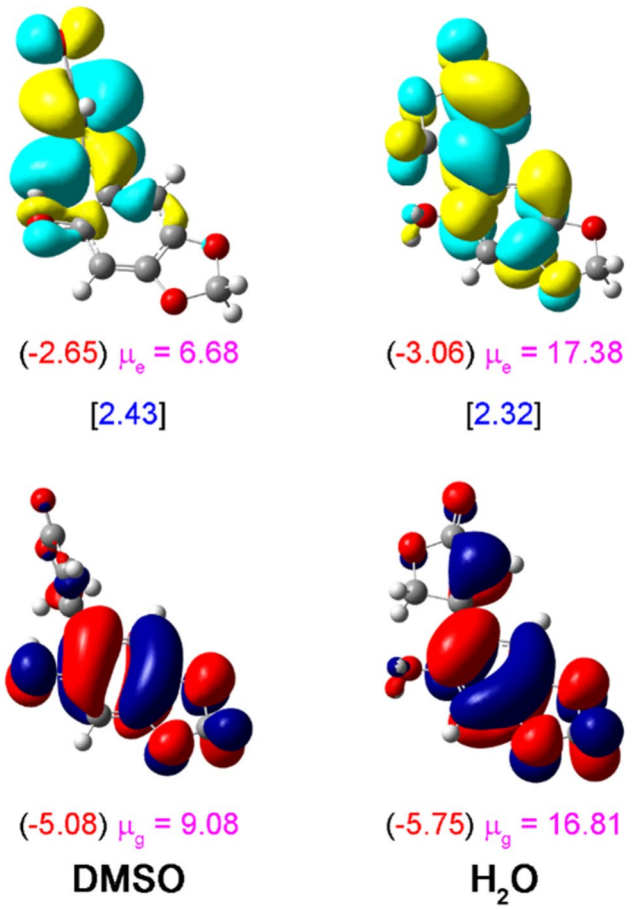


**Fig. 13** The HOMO and LUMO of **3b** in DMSO and in water. The HOMO and LUMO energies (in parenthesis), energy gaps (in square brackets) and ground ($\mu_g$) and excited state ($\mu_e$) dipole moments are shown

the molecule has the butanolide moiety twisted with the aromatic ring even before excitation. However, the mechanism involves an excited state that is less polar than the ground state [55]. The smaller dipole moment observed for **3b** in the excited state may be associated with a competition between ICT and proton-coupled electron-transfer (PCET) mechanisms that occurs through the transfer of a proton or electron [56]. According to Morawski et al. this phenomenon may be associated with the fact that in both processes, the electronic charge moves in the opposite direction to that induced by an optical excitation. As a result, the polarization of the system is partially neutralized, generating a particularly smaller dipole in the final states [56]. However, this is just a hypothesis, and further studies must be carried out to prove this statement. In water the molecule assumes a planar geometry and the dipoles moment are larger compared to those found in DMSO with μe slightly more polar than μg (Fig. 13). In water the occurrence of hydrogen bonds prevents the transfer of charge or proton. The H-bond-induced excited-to-ground-state internal conversion (IC) is the main mechanism attributed to fluorescence quenching. Numerous theoretical and experimental studies have demonstrated the strong dependence of FQY on the strength of solute–solvent H -bonds for some chromophores [57, 58, 59]. However, further studies are needed to clearly understand the fundamental origin of this H-bond-assisted non-radiative deactivation [60].

Several fluorophores, including flavone derivatives [52], 8-hydroxyquinolines [61], and tetrahydrohelicene derivatives [62] have been utilized as a basis for the development of sensors for measuring the water content in organic solvents with detection limits ranging from 0 0.0048 to 0.06% [52]. In this way, our work contributes to the efficient development of fluorescent β-(hydroxyaryl)-butenolides that exhibit fluorescence suppression in water. These properties could potentially be used for detecting water content in organic solvents or mixtures, where water may be an significant contaminant depending on the type of analysis being conducted.

DMSO is a primary solvent used for solubilizing of organic compounds in biological assays. The water content in DMSO is of great interest as it can impact solubility, degradation, and freeze–thaw cycle of compounds dissolved in this solvent [63].

Water is the most common impurity in chemical processes involving organic solvents and detection methods typically include electrochemical, advanced spectroscopic, and chromatographic methods [64]. While these methods are reliable and accurate, they have drawbacks such as lack of portability, high maintenance costs, and the need for a skilled analyst. Therefore, there is a need for the development of a more efficient and cost-effective detection method is necessary [52, 64].

## Conclusions

The synthetic probes exhibited intriguing optical properties, including high quantum yield, solvatochromism and suppression of fluorescence in water. These characteristics, along with the observed limit of detection of water in DMSO, highlight the significance of β-(hydroxyaryl)-butenolides as potential targets for the development of sensors for quickly determining of the water content in this solvent.

**Supplementary Information** The online version contains supplementary material available at https://doi.org/10.1007/s10895-023-03546-z.

**Acknowledgements** The authors thank the Fundação de Amparo à Pesquisa do Estado de São Paulo (FAPESP, process 2011/07623–8, 2018/00544-4), the Conselho Nacional de Desenvolvimento Científico e Tecnológico (CNPq, 313660/2020-4), and the Coordenação de Aperfeiçoamento de Pessoal de Nível Superior (CAPES) for scholarships and financial support. This study received partial funding from the Coordenação de Aperfeiçoamento de Pessoal de Nível Superior – Brasil (CAPES) under Finance Code 001. R.P.O., R.S.L., R.L.T.P.

and S.M.L. acknowledge the support on the Conselho Nacional de Desenvolvimento Científico e Tecnológico (CNPq) through grants 150704/2022–4, 313660/2020–4, 311122/2021–3, and 305067/2019-2 respectively.

**Author Contributions** B.F. Finêncio: Formal analysis and material preparation. F.A. Santos: Formal analysis. R.L.T. Parreira: Conceptualization, Supervision, Writing—original draft. M. Ventura: Formal analysis. R. P. Orenha: Computational methodology, Writing—original draft. S.M. Lima: Conceptualization, Supervision, Writing. L.H.C Andrade: Conceptualization, Supervision, Writing. R.S. Laurentiz: Conceptualization, Supervision, Writing—review & editing.

**Funding** The authors declare that no funds, grants, or other support were received during the preparation of this manuscript.

**Data Availability** The data set generated during the current study are available with authors.

## Declarations

**Ethical Approval** Not applicable.

**Competing Interests** The authors declare no competing interests.

## References

1. Bao Y (2021) Organic fluorescent materials as chemical sensors. Chemosensors 9:308. https://doi.org/10.3390/chemosensors9110308
2. Lu X, Zhan Y, He W (2022) Recent development of small-molecule fluorescent probes based on phenothiazine and its derivates. J Photochem Photobiol B Biol 234:112528. https://doi.org/10.1016/j.jphotobiol.2022.112528
3. Tan J, Wang C, Lao HK, Feng G, Li G, Wang W, Yuan D, Wu C, Zhang X (2019) Efficient synthesis and facile functionalization of highly fluorescent spiro[pyrrol-pyran]. Dyes Pigm 171:107777. https://doi.org/10.1016/j.dyepig.2019.107777
4. Liu H, Li X (2016) Photophysical properties of perylenetetracarboxylic diimide dimers with slipped "face-to-face" stacked structure and different bay substitutions. J Mater Sci Chem Eng 4:1–8. https://doi.org/10.4236/msce.2016.46001
5. Abreu MP, Nunes AC, Coelho FL, Campo LF (2019) Highly conjugated streptocyanine-ESIPT dyes via Vilsmeier-Haack reagent. J Lumin 213:98. https://doi.org/10.1016/j.jlumin.2019.04.063
6. Santos FA, Tondato WN, Parreira RLT, Orenha RP, Lourenço LCL, Laurentiz RS (2020) Synthesis and luminescent properties of new naphthoquinoline lactone derivatives. J Lumin 227:117547. https://doi.org/10.1016/j.jlumin.2020.117547
7. Tabuchi A, Hayakawa T, Kuwata S, Ishige R, Ando S (2021) Full-colour solvatochromic fluorescence emitted from a semi-aromatic imide compound based on ESIPT and anion formation. Mater Adv 2:5629. https://doi.org/10.1039/D1MA00308A
8. Ji F, Wu Z, Wang M, Guo Y, Wang C, Wang S, Zhao G (2022) New insights into the excited state intramolecular proton transfer (ESIPT) competition mechanism for different intramolecular hydrogen bonds of Kaempferol and Quercetin in solution. J Lumin 248:118914. https://doi.org/10.1016/j.jlumin.2022.118914
9. Zheng M, Li Y, Zhang Y, Xie Z (2016) Solvatochromic fluorescent carbon dots as optic noses for sensing volatile organic compounds. RSC Adv 6:83501. https://doi.org/10.1039/C6RA16055G
10. Zhao J, Dong H, Yang H, Zheng Y (2019) Solvent-polarity-dependent excited-state behavior and thermally active delayed fluorescence for triquinolonobenzene. ACS Appl Bio Mater 2:2060. https://doi.org/10.1021/acsabm.9b00088
11. Anandhan K, Ceróna M, Perumal V et al (2019) Solvatochromism and pH effect on the emission of a triphenylimidazole-phenylacrylonitrile derivative: experimental and DFT studies. RSC Adv 9:12085. https://doi.org/10.1039/C9RA01275C
12. Dobretsov GE, Syrejschikova TI, Smolina NV (2014) On mechanisms of fluorescence quenching by water. Biophys 59:183. https://doi.org/10.1134/S0006350914020079
13. Maillard J, Klehs K, Rumble C, Vauthey E, Heilemann M, Fürstenberg A (2021) Universal quenching of common fluorescent probes by water and alcohols. Chem Sci 12:1352. https://doi.org/10.1039/D0SC05431C
14. Bisballe N, Laursen BW (2020) What is best strategy for water soluble fluorescence dyes?—A case study using long fluorescence lifetime DAOTA dyes. Eur J Chem 26:15969. https://doi.org/10.1002/chem.202002457
15. Jung HS, Verwilst P, Kim WY, Kim JS (2016) Fluorescent and colorimetric sensors for the detection of humidity or water content. Chem Soc Rev 45:1242. https://doi.org/10.1039/C5CS00494B
16. Naidoo D, Pošta M, Roy A, Kulkarni M, Staden JV (2019) Synthesis of potent neuroprotective butenolides based on plant smoke derived 3,4,5-Trimethylfuran-2(5H)-one and 3-methyl-2H-furo[2,3-c]pyrone-2-one. Phytochem 163:187. https://doi.org/10.1016/j.phytochem.2019.03.014
17. Vallet M, Chong YM, Tourneroche A et al (2020) Novel α-hydroxy γ-butenolides of kelp endophytes disrupt bacterial cell-to-cell signaling. Front Mar Sci 7:601. https://doi.org/10.3389/fmars.2020.00601
18. Bedir E, Karakoyun Ç, Doğan G, Kuru G, Küçüksolak M, Yusufoğlu H (2021) New cardenolides from biotransformation of gitoxigenin by the endophytic fungus *Alternaria eureka* 1E1BL1: characterization and cytotoxic activities. Molecules 26:3030. https://doi.org/10.3390/molecules26103030
19. Gao M, Lee SB, Lee JE et al (2022) Anti-inflammatory butenolides from a marine-derived Streptomyces sp. 13G036. App Sci 12:4510. https://doi.org/10.3390/app12094510
20. Chaterjee S, Sahoo R, Nanda S (2021) Recent reports on the synthesis of γ-butenolide, γ-alkylidenebutenolide frameworks, and related natural products. Org Biomol Chem 19:7298. https://doi.org/10.1039/D1OB00875G
21. Tadiparthi K, Venkatesh S (2022) Synthetic approaches toward butenolide-containing natural product. J Heterocycl Chem 59:1285. https://doi.org/10.1002/jhet.4480
22. He B, Luo W, Hu S, Chen B, Zhen S, Nie H, Zhao Z, Tang BZ (2017) Synthesis and photophysical properties of new through-space conjugated luminogens constructed by folded tetraphenylethene. J Mater Chem C 5:12553. https://doi.org/10.1039/C7TC04626J
23. Lea MR, StavrosVG, Maurer RJ (2022) Effect of electron donating/withdrawing groups on molecular photoswitching of functionalized hemithioindigo derivatives: a computational multireference study. ChemPhotoChem 6:e202100290. https://doi.org/10.1002/cptc.202100290
24. Finêncio BM, Santos FA, Laurentiz RS (2023) Synthesis of β-arylbutenolides mediated by $BF_3.OMe_2$. Synlett 34:77. https://doi.org/10.1055/s-0042-1753061
25. Bhattacharyya A, Guchhait MSC, N, (2019) Photophysical properties of an azine-linked pyrene–cinnamaldehyde hybrid: evidence of solvent-dependent charge-transfer-coupled excimer emission. ACS Omega 4:2178. https://doi.org/10.1021/acsomega.8b02717
26. Chen L, Fu PY, Wang HP, Pan M (2021) Excited-state intramolecular proton transfer (esipt) for optical sensing in solid state. Adv Opt Mater 9:2001952. https://doi.org/10.1002/adom.202001952

27. Shen J, Lowe RD, Snook RD (1992) A model for cw laser induced mode-mismatched dual-beam thermal lens spectrometry. Chem Phys 165:385. https://doi.org/10.1016/0301-0104(92)87053-C
28. Lima SM, Sampaio JA, Catunda T, Bento AC, Miranda LCM, Baesso ML (2000) Mode-mismatched thermal lens spectrometry for thermo-optical properties measurement in optical glasses: a review. J Non-Cryst Solids 273:215. https://doi.org/10.1016/S0022-3093(00)00169-1
29. Becke AD (1998) Density-functional exchange-energy approximation with correct asymptotic behavior. Phys Rev A 38:3098. https://doi.org/10.1103/PhysRevA.38.3098
30. Lee C, Yang W, Parr RG (1988) Development of the Colle-Salvetti correlation-energy formula into a functional of the electron density. Phys Rev B 37:785. https://doi.org/10.1103/PhysRevB.37.785
31. Miehlich B, Savin A, Stoll H (1989) Preuss H Results obtained with the correlation energy density functionals of becke and Lee. Yang and Parr Chem Phys Lett 157:200. https://doi.org/10.1016/0009-2614(89)87234-3
32. Grimme S, Antony J, Ehrlich S, Krieg H (2010) A consistent and accurate ab initio parametrization of density functional dispersion correction (DFT-D) for the 94 elements H-Pu. J Chem Phys 132:154104. https://doi.org/10.1063/1.3382344
33. Weigend F, Ahlrichs R (2005) Balanced basis sets of split valence, triple zeta valence and quadruple zeta valence quality for H to Rn: design and assessment of accuracy. Phys Chem Chem Phys 7:3297. https://doi.org/10.1039/B508541A
34. Neese F (2003) An improvement of the resolution of the identity approximation for the formation of the Coulomb matrix. J Comput Chem 24:33051740. https://doi.org/10.1002/jcc.10318
35. Neese F, Wennmohs F, Hansen A, Becker U (2009) Efficient, approximate and parallel Hartree-Fock and hybrid DFT calculations. A 'chain-of-spheres' algorithm for the Hartree-Fock exchange. Chem Phys 356:98. https://doi.org/10.1016/j.chemphys.2008.10.036
36. Weigend F (2006) Accurate Coulomb-fitting basis sets for H to Rn. Phys Chem Chem Phys 8:1057. https://doi.org/10.1039/B515623H
37. Izsák R (2020) A local similarity transformed equation of motion approach for calculating excited states. Int J Quantum Chem 121:e26327. https://doi.org/10.1002/qua.26327
38. Berraud-Pache R, Neese F, Bistoni G, Izsak R (2020) Unveiling the photophysical properties of boron-dipyrromethene dyes using a new accurate excited state coupled cluster method. J Chem Theory Comput 16:564. https://doi.org/10.1021/acs.jctc.9b00559
39. Marenich AV, Cramer CJ, Truhlar DG (2009) Universal solvation model based on solute electron density and on a continuum model of the solvent defined by the bulk dielectric constant and atomic surface tensions. J Phys Chem B 113:6378. https://doi.org/10.1021/jp810292n
40. Neese F (2012) The ORCA program system. WIREs Comput Mol Sci 2:73. https://doi.org/10.1002/wcms.81
41. Tomasi J, Mennucci B, Cammi R (2005) Quantum mechanical continuum solvation models. Chem Rev 105:2999
42. Frisch MJ, Trucks GW, Schlegel HB., Scuseria GE., Robb MA, Cheeseman JR, Scalmani G, Barone V, Petersson, GA, Nakatsuji H, Li X, Caricato M, Marenich AV, Bloino J, Janesko BG, Gomperts R, Mennucci B, Hratchian HP, Ortiz JV, Izmaylov AF, Sonnenberg JL, Williams-Young D, Ding F, Lipparini F, Egidi F, Goings J, Peng B, Petrone A, Henderson T, Ranasinghe D, Zakrzewski VG, Gao J, Rega N, Zheng G., Lian W, Hada M, Ehara M, Toyota K, Fukuda R, Hasegawa, J., Ishida, M, Nakajima T, Honda Y, Kitao O, NakaiH, Vreven T, Throssell K, Montgomery JA Jr, Peralta JE, Ogliaro F, Bearpark MJ, Heyd JJ, Brothers EN, Kudin KN, Staroverov VN, Keith TA, Kobayashi R, Normand J, Raghavachari K, Rendell AP, Burant JC, Iyengar SS, Tomasi J, Cossi M, Millam JM, Klene M, Adamo C, Cammi R, Ochterski JW, Martin RL, Morokuma K, Farkas O, Foresman JB, Fox DJ (2016) Gaussian 16, Revision C.01. Gaussian, Inc., Wallingford CT
43. Shen Y, Chen P, Liu J, Ding J, Xue P (2018) Effects of electron donor on luminescence and mechanochromism of D-π-A benzothiazole derivatives. Dyes Pigm 150:354. https://doi.org/10.1016/j.dyepig.2017.12.034
44. Wang KY, Chen C, Liu JF, Wang Q, Chang J, Zhu HJ, Li C (2012) Novel multifunctional organic semiconductor materials based on 4,8-substituted 1,5-naphthyridine: synthesis, single crystal structures, opto-electrical properties and quantum chemistry calculation. Org Biomol Chem 10:6693–6704. https://doi.org/10.1039/C2OB25926E
45. Zhang T, Han Y, Liang M, Bian W, Zhang Y, Li X, Zhang C, Xue P (2019) Substituent effect on photophysical properties, crystal structures and mechanochromism of D-π-A phenothiazine derivatives. Dyes Pigm 171:107692. https://doi.org/10.1016/j.dyepig.2019.107692
46. Nigam S, Rutan S (2001) Principles and Applications of Solvatochromism. Appl Spectrosc 55:362A. https://doi.org/10.1366/0003702011953702
47. Divya TT, Ramshad K, Saheer VC, Chakkumkumarath L (2018) Self-reversible mechanochromism and aggregation induced emission in neutral triarylmethanes and their application in water sensing. New J Chem 42:20227. https://doi.org/10.1039/c8nj04479a
48. Wie NN, Hao C, Xiu Z, Qiu J (2010) Time-dependent density functional theory study on the coexistent intermolecular hydrogen-bonding and dihydrogen-bonding of the phenol-$H_2O$-diethylmethylsilane complex in electronic excited states. Phys Chem Chem Phys 12:9445. https://doi.org/10.1039/B927049C
49. Zhao GJ, Liu JY, Zhou LC, Han KL (2007) Site-selective photoinduced electron transfer from alcoholic solvents to the chromophore facilitated by hydrogen bonding: a new fluorescence quenching mechanism. J Phys Chem B 111:8940. https://doi.org/10.1021/jp0734530
50. Ghosh HN, Verma S, Nibbering ETJ (2011) Ultrafast forward and backward electron transfer dynamics of coumarin 337 in hydrogen-bonded anilines as studied with femtosecond UV-pump/IR-probe spectroscopy. J Phys Chem A 115:664. https://doi.org/10.1021/jp108090b
51. Li Q, Li Z (2017) The strong light-emission materials in the aggregated state: what happens from a single molecule to the collective group. Adv Sci 4:1600484. https://doi.org/10.1002/advs.201600484
52. Kumar P, Ghosh A, Jose DA (2021) Chemical sensors for water detection in organic solvents and their applications. Chem Sel 6:820. https://doi.org/10.1002/slct.202003920
53. Lakowicz JR (2006) Principles of Fluorescence Spectroscopy. 3rd Edition, Springer, Berlin. https://doi.org/10.1007/978-0-387-46312-4
54. Algar WR, Massey M (2019) Key errors to avoid in the consideration of fluorescence quenching data. Spectrosc Suppl 34:12
55. Sinha HK, Muralidharan S, Yate K (1992) Ground and excited state dipole moments of planar vs. twisted p-N, N-(dimethy1amino)benzonitrile systems: maximum charge transfer for minimum overlap. Can J Chem 70:1932. https://doi.org/10.1139/v92-24
56. Morawski OW, Kielesiński Ł, Gryko DT, Sobolewski AL (2020) Highly polarized coumarin derivatives revisited: solvent-controlled competition between proton-coupled electron transfer and twisted intramolecular charge transfer. Chem Eur J 26:7140. https://doi.org/10.1002/chem.202001079
57. Lopez Arbeloa T, Lopez Arbeloa F, Tapia MJ, Lopez Arbeloa I (1993) Hydrogen-bonding effect on the photophysical properties of 7-aminocoumarin derivatives. J Phys Chem 97:4704. https://doi.org/10.1021/j100120a024

58. Sobolewski AL, Domcke W (2007) Computational studies of the photophysics of hydrogen-bonded molecular systems. J Phys Chem A 111:11725. https://doi.org/10.1021/jp075803o
59. Zhao GJ, Han KL (2009) Role of intramolecular and intermolecular hydrogen bonding in both singlet and triplet excited states of aminofluorenones on internal conversion, intersystem crossing, and twisted intramolecular charge transfer. J Phys Chem A 113:14329. https://doi.org/10.1021/jp903200x
60. Kim JS, Choi MG, Huh Y, Kim SH, Wang SY, Chang SK (2006) Determination of water content in aprotic organic solvents using 8-hydroxyquinoline based fluorescent probe. Bull Korean Chem Soc 27:2058. https://doi.org/10.5012/bkcs.2006.27.12.2058
61. Chen C, Fang C (2023) Fluorescence modulation by amines: mechanistic insights into twisted intramolecular charge transfer (TICT) and beyond. Chemosensors 11:87. https://doi.org/10.3390/chemosensors11020087
62. Cai L, Sun X, He W, Hu R, Liu B, Shen J (2020) A solvatochromic AIE tetrahydro[5]helicene derivative as fluorescent probes for water in organic solvents and highly sensitive sensors for glyceryl monostearate. Talanta 206:120214. https://doi.org/10.1016/j.talanta.2019.120214
63. Semin DJ, Malone TJ, Paley MT, Woods PW (2005) A novel approach to determine water content in DMSO for a compound collection repository. J Biomol Screen 10:568. https://doi.org/10.1177/1087057105276369
64. Liu YC, Lu GD, Zhou JH, Rong JW, Liu HY, Wang HY (2022) Fluoranthene dyes for the detection of water content in methanol. RSC Adv 12:7405. https://doi.org/10.1039/D1RA08392A